JOURNAL OF AGRICULTURAL AND FOOD CHEMISTRY

Iron Chelation by the Powerful Antioxidant Flavonoid Quercetin

MONICA LEOPOLDINI, NINO RUSSO,* SANDRO CHIODO, AND MARIROSA TOSCANO

Dipartimento di Chimica and Centro di Calcolo ad Alte Prestazioni per Elaborazioni Parallele e Distribuite-Centro d'Eccellenza MIUR, Università della Calabria, I-87030 Arcavacata di Rende (CS), Italy

Chelation of the bare and hydrated iron(II) cation by quercetin has been investigated at the DF/B3LYP level in the gas phase. Several complexed species arising from neutral and anionic forms of the ligand have been taken into account. Both 1:1 and 1:2 metal/flavonoid stoichiometries have been considered. Results indicate that among the potential sites of chelation present on quercetin, the oxygen atoms belonging to the 3-hydroxy and 4-oxo, and to the 5-hydroxy and 4-oxo groups, are the preferred ones. Time-dependent density functional theory (TDDFT) calculations, used to reproduce the electronic UV−vis spectra of isolated quercetin and its complexes with Fe^{2+}, were also performed in methanol and dimethylsulfoxide.

KEYWORDS: Quercetin; iron(II); complexation; antioxidants

INTRODUCTION

Plants, in response to external environmental causes, synthesize and accumulate a great variety of natural products such as alkaloids, flavonoids, and terpenoids (*1*). These compounds serve as defensive and protective agents. For instance, they act as shields against UV light, attractants for pollination and ovoposition, signals for N-fixating bacteria, and antimicrobial/antiviral agents (*1*).

Flavonoids are polyphenolic compounds mainly found in fruits, vegetables, and cereals (*2*). Interest in these compounds has grown in consequence of epidemiological and biochemical studies that have highlighted their numerous properties such as antioxidant activity (*3*), inhibition of tyrosine chinases (*4*) and cAMP phosphodiesterase (*5*), induction of phase II metabolizing enzymes (*6*), control of cellular growth (*7*), destruction of pathogen organisms (fungi and viruses) (*8*), and inhibition of human immunodeficiency virus (HIV) transcriptase and HIV replication (*9*). Many dietary polyphenolics are more effective antioxidants in vitro than vitamins E and C, and they are associated with a minor incidence of cancer (*10*−*12*).

Quercetin is a member of a flavonoids class characterized by a flavone nucleus composed of two benzene rings linked through a heterocyclic pyrone ring (see **Scheme 1**). It mainly occurs in apples, onions, tea, red wines, and berries.

Experimental studies demonstrated that it possesses numerous beneficial effects on human health, including cardiovascular protection, anticancer activity, antiulcer effects, and antiallergic, antiviral, and anti-inflammatory properties. Many of these effects are correlated to antioxidant capability that is due to the scavenging of free radicals species and to synergistic effects with enzymes and physiological antioxidants (*13*−*24*).

In the literature, two main mechanisms by which antioxidants can play their protective role were proposed and widely analyzed

Scheme 1

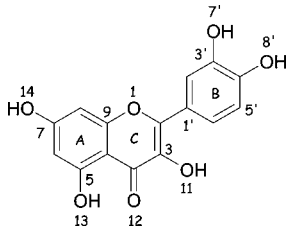

(*25*−*27*). The H-atom transfer, in which a free radical $R^{\bullet}$ removes an hydrogen atom from the antioxidant (ArOH):

$$R^{\bullet} + ArOH \rightarrow RH + ArO^{\bullet}$$

and the one-electron transfer mechanism, according to which the antioxidant can give an electron to the free radical:

$$R^{\bullet} + ArOH \rightarrow R^{-} + ArOH^{\bullet +}$$

The radicals arising from both reactions ($ArO^{\bullet}$ and $ArOH^{\bullet +}$) must be stable to prevent or delay chain radical reactions.

Another antioxidant mechanism, not exhaustively studied, is based on the ability of some of these compounds to chelate transition metals ions (especially iron and copper), giving rise to stable complexes that, entrapping metals, prevent these from participating in free radicals generation (*28*). In fact, during the Fenton reaction (*29*, *30*), hydroxyl radicals are produced from hydrogen peroxide in the presence of a metal in a low oxidation state:

$$H_2O_2 + M^{n+} \rightarrow HO^{-} + HO^{\bullet} + M^{(n+1)+}$$

Fenton chemistry may occur in dopaminergic neurons of nervous tissue where normally dopamine catabolism produces

* To whom correspondence should be addressed. E-mail: nrusso@unical.it.

10.1021/jf060986h CCC: $33.50
Published on Web 08/02/2006

some level of hydrogen peroxide (*31*). The accumulation of free radicals in these neurons may be recognized as the main etiological agent of Parkinson disease (*31*).

Metal-chelating compounds remove the metals and can alter their redox potentials rendering them inactive. Moreover, the use of natural metal chelators such as flavonoids should be favored against other synthetic chelators which may present some problems of toxicity.

Flavonoids, with their multiple hydroxyl groups and the carbonyl group on ring C, have several available sites for metal complexation. Many experimental (*32*−*37*) and theoretical (*38*−*45*) works were devoted to quercetin, including conformational and electronic structure determinations, and spectroscopic and X-ray analyses. However, few investigations have concerned the formation of stable complexes between quercetin and transition metals ions (*46*−*50*). Among the different 1:1, 1:2, 2:2, 2:3 stoichiometries that metal/flavonoid complexes can exhibit, the 1:2 is the preferred one (*47*). Electrospray ionization mass spectrometry (ESI-MS) studies (*50*) indicated that the preferred complexation site for flavonoids is that involving the hydroxyl at carbon 3 or 5 and the adjacent 4-carbonyl group. Experiments in aprotic medium (*49*) revealed that both neutral and anionic quercetin forms 1:1 complexes with iron(II). Cornard and co-workers (*45*, *51*) investigated the complexation of Al(III) and Pb(II) ions by quercetin. In their theoretical study, they concluded that the preferential coordination sites of quercetin are the 3-hydroxy chromone moiety and the catechol group, for aluminum and lead ion, respectively.

Here, we present a detailed DF-B3LYP study on the chelation of iron(II) by quercetin, considering both the neutral and deprotonated species of quercetin and the bare and hydrated Fe^{2+} cation. The aim was the determination of the electronic and structural features of the iron−quercetin complexes to identify the most likely species responsible for the antioxidant action.

EXPERIMENTAL PROCEDURES

The DFT computations were performed using the Gaussian03 quantum chemical package (*52*). Geometry optimization of quercetin, its anions, and all their 1:1 and 1:2 complexes with the bare and hydrated iron cation was carried out using the Becke3 (*53*) and Lee Yang Parr (*54*) (B3LYP) hybrid functional. The 6-31G* basis set (*55*−*58*), and the LANL2DZ (*59*) pseudopotential, were chosen for C, O, and H atoms, and for Fe^{2+} cation, respectively.

Minima and saddle points were identified through frequency calculations performed at the same level of theory. Zero point energy corrections, obtained from vibrational analysis, were then included in all the relative energy values.

Geometry optimization was followed by single-point calculations using the extended 6-311++G** basis set for the nonmetal atoms to refine electronic energies.

Natural bond orbital (NBO) analysis implemented in the Gaussian03 package was used to better characterize the metal ion−ligand bond nature.

The UV−vis spectra of free and complexed quercetin were obtained as vertical excitation energies using the time-dependent density functional theory (TDDFT) (*60*) implemented in the Gaussian03 code with the B3LYP/6-31G*/LANL2DZ protocol.

Solvent effects on UV−vis spectra were computed in the framework of the self-consistent reaction field polarizable continuum model (SCRF-C-PCM) (*61*−*63*) using the simple united atom topological model (UAO) (*64*) set of solvation radii to build the cavity for the solute in its gas-phase equilibrium geometry. The dielectric constants of 32.6 and 46.7 were chosen to perform computations in methanol and in dimethylsulfoxide, respectively.

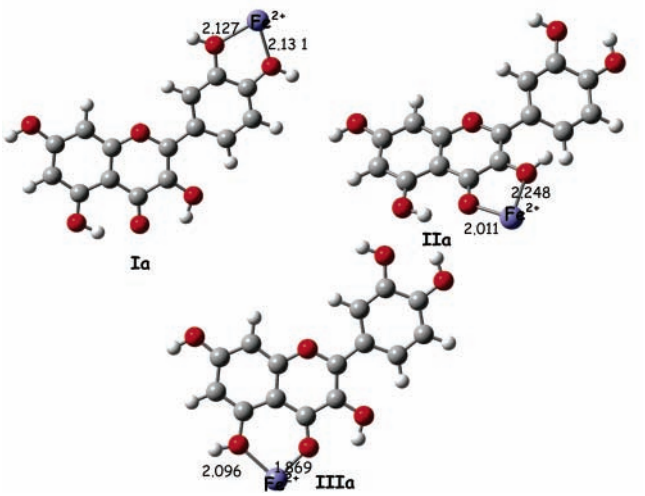

Figure 1. Optimized geometries of iron–quercetin (1:1 ratio) complexes Ia, IIa, and IIIa.

Table 1. Relative Energies, Including ZPE Corrections (ΔE in kcal/mol), of Fe(II)–Quercetin Complexes[a]

species	ΔE	species	ΔE	species	ΔE	species	ΔE	species	ΔE
Ia	12.3	Ib	27.4	Ic	13.8	Id	0.0	Ie	12.9
IIa	10.1	IIb	23.6	IIc	12.9	IId	5.9	IIe	5.2
IIIa	0.0	IIIb	5.6	IIIc	0.0	IIId	1.6	IIIe	0.0
		IVb	0.0	IVc	1.8	IVd	2.5	IVe	9.3
		Vb	34.2	Vc	41.0				
		VIb	35.3	VIc	50.5				
		VIIb	48.3	VIIc	50.5				
		VIIIb	41.7	VIIIc	42.3				

[a] *a* = complex between quercetin (Q) and Fe^{2+}; *b* = complex between deprotonated quercetin (Q^-) and Fe^{2+}, *c* = complex between Q^- and $Fe^{2+}(H_2O)_4$, *d* = complex between $2Q^-$ and Fe^{2+}; *e* = complex between $2Q^-$ and $Fe^{2+}(H_2O)_2$.

RESULTS AND DISCUSSION

Interaction between Neutral Quercetin and Bare Fe(II) Cation. Quercetin is a planar species characterized by electronic conjugation and delocalization that involve the whole molecule (*39*). The OH groups are arranged in such a way as to maximize the number of hydrogen bonds (*39*).

In principle, there are three possible sites on quercetin for the iron(II) chelation: the catechol moiety, the 3-OH and C_4═O and C_4═O and 5-OH groups. The coordination to these sites can give rise to three compounds depicted in **Figure 1**.

Global minimum is represented by the complex IIIa that lies 12.3 and 10.1 kcal/mol below the Ia and IIa species, respectively (see **Table 1**). In the lowest energy system, iron ion coordinates both the oxygen atoms of the C_4═O carbonyl (1.869 Å) and the C_5−OH (2.096 Å) groups with the formation of a six-membered ring coplanar with the rest of the molecule. The value of the dihedral angle Ψ (179.9°) between C and B rings indicates that the planarity is retained in going from free to complexed quercetin.

In complex IIa, Fe^{2+} establishes two coordination bonds with the C_3-OH and 4-keto groups oxygen atoms. Fe^{2+}−OH and Fe^{2+}−O═C lengths are 2.248 and 2.011 Å, respectively. In these compounds, the cation complexation withdraws electron density to the metalation site and avoids π electrons delocalization from ring C to ring B, as the value of the Ψ torsional angle (153.1°) indicates.

Finally, the species Ia is characterized by the formation of a five-membered cycle involving the metal and the oxygen atoms

of $C_{3'}-OH$ and $C_{4'}-OH$ hydroxyls (distances are 2.127 and 2.131 Å, respectively). The relative energy of the last complex confirms the poor iron chelating power of the catechol group (*46*, *49*).

NBO analysis, performed for the most likely IIIa species, shows that Fe^{2+} forms a purely ionic bond with hydroxyl oxygen. The charge transfer from the ligand to metal ion of 0.7 |e| underlines the presence of a covalent contribution that we find in the bond formed with the carbonyl oxygen. The molecular orbital responsible for the covalent bond arises from the 2p and 3d orbitals of oxygen and iron, respectively.

Interaction between Deprotonated Quercetin and Bare and Hydrated Fe(II) Cation. The OH groups of flavonoids are slightly acidic (*65*), so that they may exist in some anionic form at physiological pH values. The quercetin anions are all planar systems. Natural net charges and bond order values lead us to argue that in all anions the negative charge is widely delocalized over two rings: from ring A to ring C or from ring B to ring C, in the case of 5-OH and 7-OH, and 4′-OH and 3-OH anions, respectively (*65*). The only exception is the 3′-OH species in which the lone pair is confined on the deprotonation site. The deprotonation of the 4′-OH group yields to the most stable anion that is characterized by an internal hydrogen bond. The other anions are found at 6.8 (3′-OH), 16.6 (3-OH), 20.9 (5-OH), and 6.0 (7-OH) kcal/mol above the former. The energetic gaps among the anionic species of quercetin are sensibly lower in water solution where the 3′-OH one becomes the global minimum. The other species follow at 1.6 (4′-OH), 1.5 (3-OH), 4.0 (5-OH), and 1.7 (7-OH) kcal/mol. These latter results indicate that all the anions of quercetin may coexist in vivo.

Fe^{2+} attack may occur not only on the deprotonation sites but also on the other positions that originate from resonance effects; thus, the complexed species are quite numerous (see **Figure 2**).

B3LYP computations indicate as a global minimum the adduct IVb in which the cation is coordinated to the carbonyl oxygen on ring C and to the deprotonated 5-OH hydroxyl (**Figure 2**). The coordination bonds established with the carbonyl and hydroxyl oxygen atoms are of 1.869 and 1.813 Å, respectively.

The complex IIIb lies at 5.6 kcal/mol above the global minimum (**Table 1**). In this case, the Fe^{2+} cation is coordinated to the $C_4{=}O$ and to the deprotonated 3-OH groups. A five-membered ring coplanar with the rest of the molecule is formed.

The other complexes are found at 27.4 (1b), 23.6 (IIb), 34.2 (Vb), 35.3 (VIb), 48.3 (VIIb), and 41.7 (VIIb) kcal/mol above the IVb one. As it can be seen from the equilibrium geometries reported in **Figure 2**, when iron(II) is coordinated to the 3-OH and $C_4{=}O$ groups, the torsional angle $C_3-C_2-C_{1'}-C_{2'}$ moves away from the planarity ($\Psi = 145.7°$ and 146.6°, for complexes Vb and VIIb, respectively).

The results concerning the relative energies of complexes Ib and IIb indicate again a scarce chelating ability of catechol toward the iron cation.

On the basis of the evidence that flavones lacking the carbonyl and hydroxyl pair produce the lowest intensities in ESI-MS signals (*50*), experimentalists suggested that the coordination of transition metals by flavonoids anions occurs via their oxygen atoms at carbon 3 and carbon 4 or carbon 4 and carbon 5. The same conclusions were deduced (*46*, *47*) from electronspray mass spectrometry studies on some transition metals flavonoids complexes. Furthermore, the complexation at the 4-carbonyl and 5-OH groups was recognized as the preferred one.

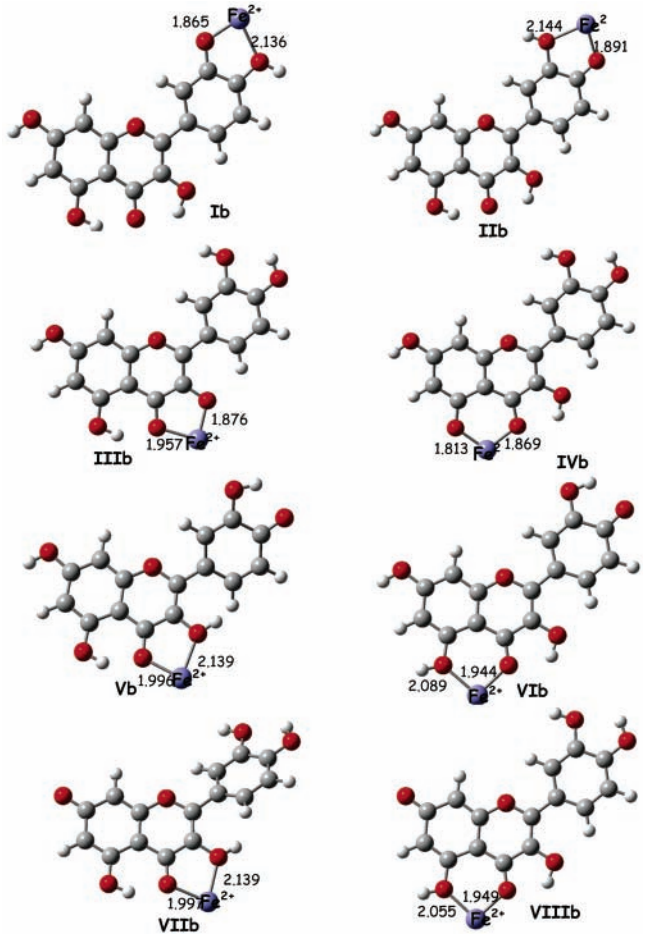

Figure 2. Optimized geometries of iron–deprotonated quercetin (1:1 ratio) complexes Ib, IIb, IIIb, IVb, Vb, VIb, VIIb, and VIIIb.

NBO analysis indicates a charge transfer of 0.5 |e| from ligand to cation. This means that the ionic character on the whole increases with respect to the previous case. In particular, Fe^{2+} forms with deprotonated oxygen a ionic bond with a small covalent contribution arising from the overlap between the 2p orbital of oxygen and the 3d orbital of the metal center. The bond with carbonyl oxygen is essentially ionic.

In physiological liquids, the Fe^{2+} cation should be present as an aquocomplex with a variable number of coordinating water molecules. Usually, iron(II) forms hydrated complexes in which the preferred coordination around the cation is of the octahedral type.

For these reasons, four water molecules were added to the coordination sphere of Fe^{2+} in all complexes of *b* type, obtaining the corresponding minima structures Ic−VIIIc, whose equilibrium geometries are reported in **Figure 3**.

As can be noted, all water molecules were retained after optimization. The presence of water causes a stability inversion between the III and IV species.

Among the complexes of hydrated ion, the global minimum is the IIIc adduct. In this system, the bond lengths between cation and carbonyl and deprotonated 3-OH oxygen atoms are 2.015 and 2.073 Å, respectively. Furthermore, the torsional angle value ($\Psi = 164.1$) indicates a deviation from the planarity.

In complex IVc, which lies at 1.8 kcal/mol above IIIc, the distances of hydrated Fe^{2+} from the oxygen atoms belonging to carbonyl and deprotonated 5-OH hydroxyl were found to be 2.047 and 1.940 Å, respectively.

The species Ic and IIc characterized by the coordination at the catechol moiety, lie at 13.8 and 12.9 kcal/mol above the

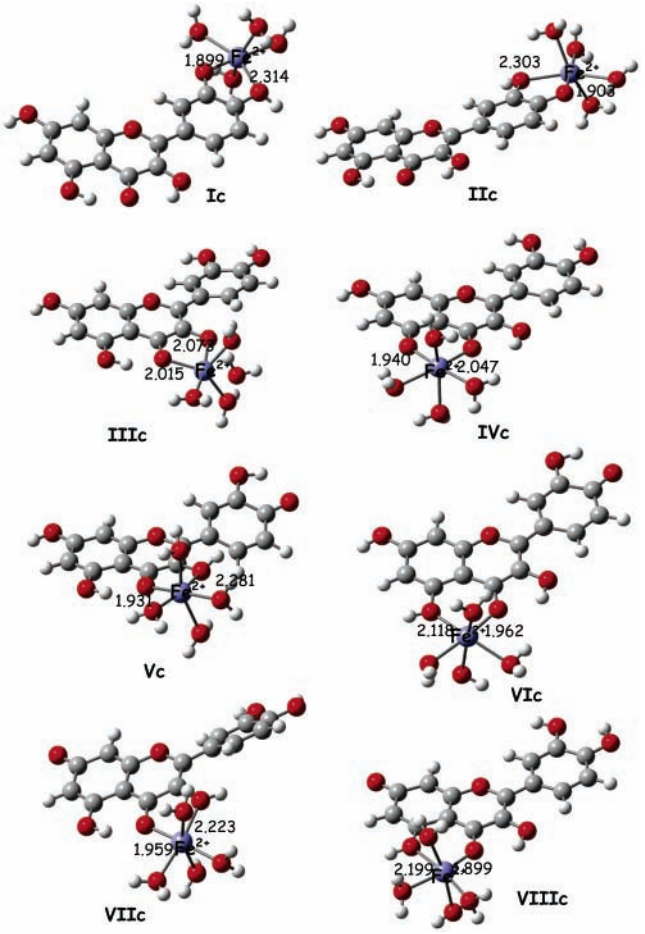

Figure 3. Optimized geometries of hydrated iron–deprotonated quercetin (1:1 ratio) complexes of Ic, IIc, IIIc, IVc, Vc, VIc, VIIc, and VIIIc.

global minimum, respectively. The remaining complexes Vc, VIc, VIIc, and VIIIc are found at very high energies (41.0, 50.5, 50.5, and 42.3 kcal/mol, respectively).

Although the presence of water molecules in the coordination sphere of Fe^{2+} reduces the energy separations between the complexes (see **Table 1**), also in this case, likewise for bare ion−quercetin complexes, only the first four species may coexist in physiological environments, while the latter four are not so relevant as iron chelates.

NBO analysis suggests that upon interaction of hydrated Fe^{2+} with quercetin anions, the natural net charge on the cation remains very similar to that computed for free aquocomplex (1.52 vs 1.62 |e|). This means that a ionic bond is present, in this case. This result is different from that concerning the complexes in which the coordination sphere of the cation is lacking in water molecules, but it is not surprising since the orbital availability to form covalent bonds decreases gradually as the coordination number of the cation increases.

Interaction between Two Deprotonated Quercetin and Bare and Hydrated Fe(II) Cation. Electronspray mass spectrometry studies (*47*) revealed that for metal ion−flavonoid complexes a number of different stoichiometries, namely, 1:1, 1:2, 2:2, 2:3, is possible, the 1:2 being the preferred one. For instance, Deng and Van Berkel observed experimentally an Al(III)−quercetin complex of 1:2 stoichiometry (*66*) in methanol solutions, and Cornard et al. (*51*) identified a 1:2 complex between aluminum and deprotonated quercetin. Thus, we were interested to investigate the formation of chelates made of two deprotonated quercetin molecules and bare and hydrated Fe^{2+}.

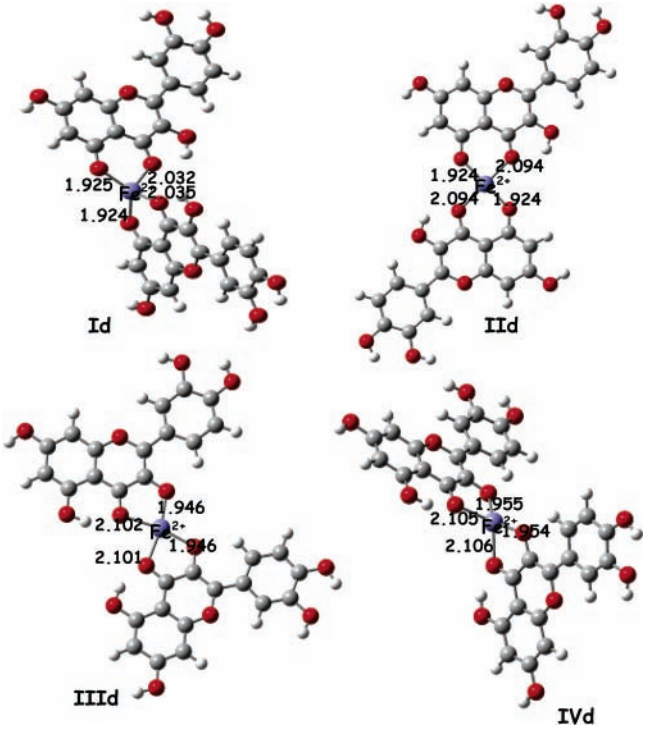

Figure 4. Optimized geometries of iron–deprotonated quercetin (1:2 ratio) complexes Id, IId, IIId, and IVd.

Taking into account that *a*, *b*, and *c* iron(II)−quercetin most stable adducts are obtained as the oxygen atoms linked to carbon 3−carbon 4 and carbon 4−carbon 5 pairs, we considered only the complexes arising from the interaction with the 3-OH and 5-OH anions.

The "cis" and "trans" orientations of the two quercetin anions around the cation were examined.

The relative energies of the four obtained species Id, IId, IIId, and IVd depicted in **Figure 4** are reported in **Table 1**.

The global minimum is represented by the Id complex originated by the interaction with the 5-OH anions in the "cis" position. The coordination geometry around the cation is tetrahedral and involves two carbonyl O_{12} (2.035 and 2.032 Å) and two hydroxyl O_{13} (1.924 and 1.925 Å) atoms.

The other three species lie at 1.6 (IIId), 2.5 (IVd), and 5.9 (IId) kcal/mol above the most stable one.

Computations show that the "cis" arrangement of quercetin anions is energetically favored with respect to the "trans" one. The tetrahedral coordination (structures Id and IVd) is favored with respect to the square planar geometry (IId and IIId). These statements seem to be in disagreement with the energetic trend reported in **Table 1** because of the larger stability of species IIId with respect to the complex IVd. Really, the lower energy of IIId can be attributed to the presence of two strong $O_{13}H-O_{12}$ hydrogen bonds (1.776 Å) that are much less intense in the other structures.

The charge on the iron ion in the Id complex is 1.41 |e|. This value suggests a charge transfer from ligand to cation. NBO analysis indicates the presence of two covalent bonds between Fe^{2+} and the oxygen atom of both deprotonated 5-OH groups. Overlap involves the two hybrid s(11.30%)p(88.7%) and s(19.00%)d(81%) orbitals of oxygen and iron, respectively.

Starting from minima with bare cation, two water molecules in the coordination sphere of Fe^{2+} were added. The presence of these molecules gave rise to a quite different situation from that obtained previously. In particular, the most stable complexes are now originated from the less favored IId and IIId systems

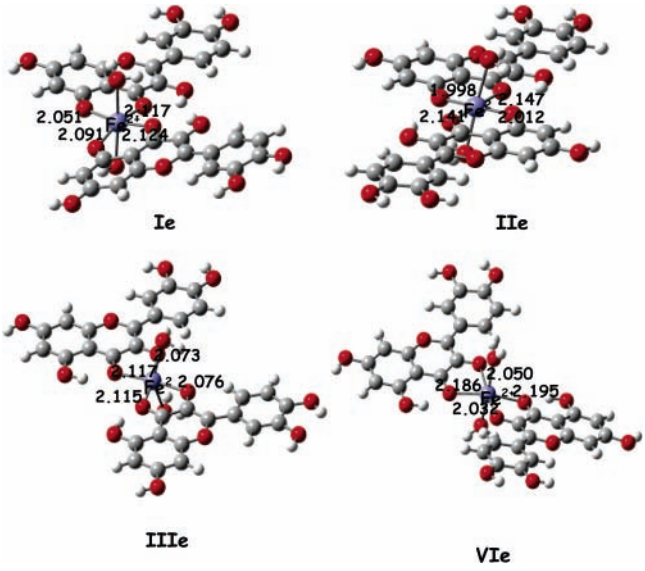

Figure 5. Optimized geometries of hydrated iron–deprotonated quercetin (1:2 ratio) complexes Ie, IIe, IIIe, and IVe.

because of their planar disposition of ligand atoms. This can be explained by considering that the final octahedral geometry is more easily reachable starting from planar complexes. In other words, the rearrangement required to pass from a tetrahedral to octahedral coordination entails a larger energy expense. Thus, in the case of a hydrated cation the global minimum is represented by the IIIe system (see **Figure 5**) in which the iron cation is coordinated by the oxygen atoms attached to C_3 and C_4 carbon atoms of two 3-OH anions in the "cis" position and by two water molecules. The two anions have similar geometrical parameters ($Fe-O_{11}$ and $Fe-O_{12}$ distances are 2.073 and 2.117 Å, and 2.076 and 2.115 Å, for the first and second anion, respectively). The ligands are completely coplanar, while the axial H_2O molecules are so arranged that a slight deviation from ideal octahedral geometry can be observed.

The analogous complex IVd having the "trans" ligands arrangement lies at 9.3 kcal/mol above the former.

The IIe species, in which two 5-OH anions in a mutual "trans" position are involved, appear to be less stable by 5.2 kcal/mol with respect to the global minimum. Also for this chelate, the ligands are coplanar, and the water molecules are staggered. $Fe-O_{12}$ and $Fe-O_{13}$ coordination distances are 2.147 and 1998 Å for one of ligands, and 2.141 and 2.012 Å for the other one, respectively.

The remaining Ie species is found at 12.9 kcal/mol with respect to the global minimum.

Results concerning the relative energy values suggest that only IIe and IIIe complexes can be relevant from a biological point of view as stable chelates of iron(II).

NBO analysis in this case confirms the ionic nature of the interaction because of the similarity between the natural charge on hydrated iron(II) before (1.62 |e|) and after the complexation (1.52 |e|).

To verify the agreement with the experimental observation concerning the predominance of the complexes having the 2:1 ligand/metal ion stoichiometry with respect to those with 1:1 one, we have computed the binding energy (BE) values for the global minima belonging to all different categories of examined systems. Values obtained for type *b*, *c*, *d*, and *e* complexes are 431.9, 517.0, 601.6, and 615.2 kcal/mol, respectively. Thus, as expected, also from a theoretical point of view, the preference for the 2:1 ratio is confirmed.

UV−vis Spectra. The experimental UV−vis spectra of free quercetin were recorded in methanol (*38*) and in dimethylsul-

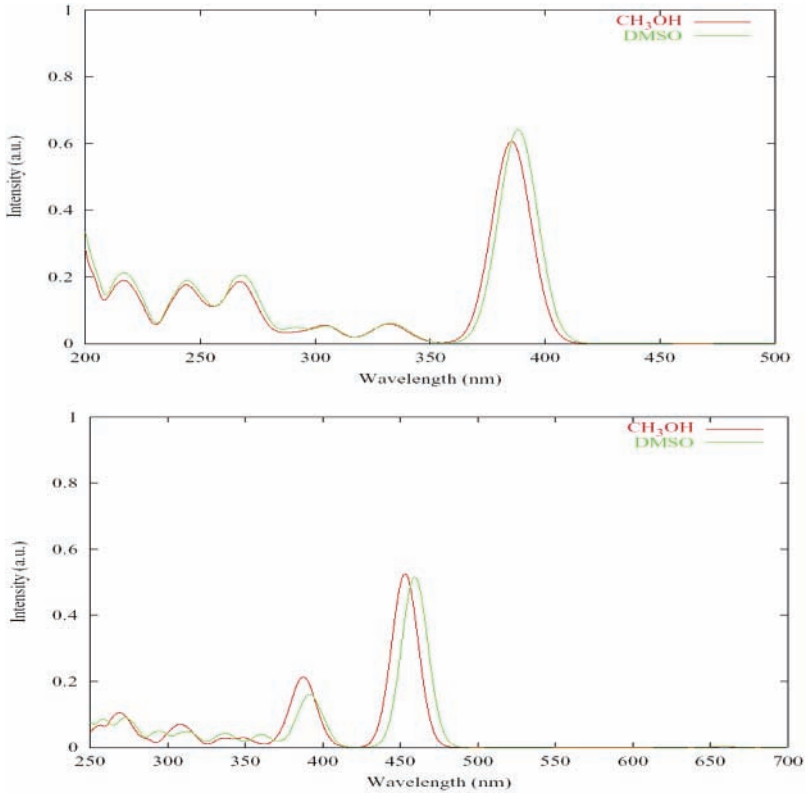

Figure 6. UV–vis spectra of free quercetin (top) and iron-deprotonated quercetin complex IVb (bottom). The graph was obtained by using Gaussian functions centered at each value of the absorption wavelength. Then the shape was adjusted by least-square fitting using a linear combination of Gaussian functions.

Table 2. Computed TDDFT Main Vertical Excitation Energies (in nm), Oscillator Strengths, and MO Contribution (%) of Free Quercetin in Methanol and DMSO Solutions

methanol		DMSO	
vertical energies (oscillator strengths)	MO contribution	vertical energies (oscillator strengths)	MO contribution
385 (0.6063)	H → L (82%)	388 (0.6408)	H → L (83%)
332 (0.0602)	H-1 → L (90%)	333 (0.0602)	H-1 → L (90%)
303 (0.0552)	H-2 → L (87%)	303 (0.0547)	H-2 → L(87%)
267 (0.1845)	H → L + 1 (56%); H-3 → L (21%)	268 (0.2054)	H → L + 1 (58%); H-3 → L (20%)
253 (0.1180)	H → L + 2 (40%); H-1 → L + 1 (30%); H-4 → L (14%)	253 (0.1225)	H → L + 2 (40%); H-1 → L + 1 (30%); H-4 → L (14%)
244 (0.1745)	H-1 → L + 1 (30%); H → L + 3 (26%); H-4 → L (15%); H-2 → L + 1 (7%); H → L + 2 (6%)	244 (0.1878)	H-1 → L + 1 (32%); H → L + 3 (23%); H-4 → L (15%); H → L + 2 (7%); H-2 → L + 1 (6%)
216 (0.1906)	H-1 → L + 2 (34%); H-2 → L + 1 (24%); H-1 → L + 3 (14%)	217 (0.2109)	H-1 → L + 2 (37%); H-2 → L + 1 (+25%); H-1 → L + 3 (14%)
210 (0.0746)	H → L + 4 (32%); H-6 → L (15%); H-2 → L + 2 (12%); H-3 → L + 3 (10%); H-4 → L + 1 (10%); H-3 → L + 2 (8%)	211 (0.0806)	H → L + 4 (31%); H-6 → L (18%); H-2 → L + 2 (12%); H-3 → L + 3 (10%); H-4 → L + 1 (8%); H-3 → L + 2 (8%)
209 (0.0967)	H-6 → L (36%); H-1 → L + 3 (25%); H-4 → L + 1 (9%); H-1 → L + 2 (9%)	209 (0.1063)	H-6 → L (33%); H-1 → L + 3 (27%); H-4 → L + 1(9%); H-1 → L + 2 (9%)
206 (0.0574)	H → L + 4 (36%); H-6 → L (15%); H-1 → L + 3 (14%); H-3 → L + 2 (9%); H-2 → L + 3 (5%)	206 (0.0605)	H → L + 4 (37%); H-6 → L (15%); H-1 → L + 3 (14%); H-3 → L + 2 (9%); H-2 → L + 3 (5%)

Table 3. Computed TDDFT Main Vertical Excitation Energies (in nm), Oscillator Strengths, and MO Contribution (%) of IVb Iron–Quercetin Complex in Methanol and DMSO Solutions

Complex IVb			
methanol		DMSO	
vertical energies (oscillator strengths)	MO contribution	vertical energies (oscillator strengths)	MO contribution
453 (0.5263)	H → Lα (41%); H → Lβ (34%); H-1 → Lα (8%)	459 (0.5161)	H → Lα (40%); H → Lβ (32%); H-1 → Lα (12%)
387 (0.2127)	H-1 → Lα (49%); H-1 → Lβ (32%)	392 (0.1584)	H-1 → Lα (38%); H-1 → Lβ (25%);
308 (0.0707)	H-4 → Lα (44%); H-4 → Lβ (26%); H-2 → L + 4β (6%); H → L + 4β (5%); H → L + 2α (5%)	273 (0.0895)	H-1 → L + 2α (17%); H → L + 2α (13%); H → L + 4α (8%); H → L + 4β (7%)
274 (0.0565)	H-2 → L + 3β (15%); H → L + 4β (14%); H → L + 3α (14%); H → L + 2α (11%); H-3 → L + 6β (8%); H-3 → L + 3α (7%); H-5 → Lα (5%)	258 (0.0842)	H-1 → L + 2α (21%); H-1 → L + 4β (19%); H-3 → L + 2β (12%); H → L + 6β (10%); H → L + 3α (8%)
269 (0.1054)	H-1 → L + 2α (20%); H-2 → L + 3β (16%); H → L + 4α (11%); H → L + 2α (7%); H → L + 8β (6%)	255 (0.0572)	H-3 → L + 2β (25%); H-1 → L + 4β (13%); H-1 → L + 2α (9%); H-4 → L + 4β (6%); H-7 → Lβ (6%); H → L + 6β (6%)
257 (0.0669)	H-2 → L + 4β (21%); H-1 → L + 2α (18%); H-7 → Lα (9%); H-7 → Lβ (8%); H → L + 3α (7%); H-6 → L + 1β (5%); H → L + 6β (5%)	250 (0.0739)	H → L + 3α (17%); H → L + 6β (13%); H-1 → L + 4β (11%); H-7 → Lα (11%) H-7 → Lβ (9%); H-3 → L + 2β (8%); H-3 → L + 2α (5%)

foxide (*49*) solutions. While the resolution of the spectrum in methanol indicates clearly an absorption band around 372 nm and another one at 255 nm with a shoulder at 269 nm (*38*), for that in dimethylsulfoxide only the shape is available. However, in this second case, a band of absorption in the region 370−390 nm can be recognized.

To provide a more complete spectroscopic characterization and for purposes of comparison, B3LYP/6-31G* spectra of free quercetin in methanol and in dimethylsulfoxide were computed and reported in **Figure 6**. The obtained vertical energies are collected in **Table 2**, together with oscillator strengths and molecular orbitals contributions involved in the transitions. The four Gouterman's orbitals (HOMO-1, HOMO, LUMO, and LUMO+1) for quercetin and the iron−quercetin complex IVb are depicted in **Figure 7**.

The HOMO of free quercetin presents a charge density localized mainly on the ring B and on the C_2-C_3 double bond in the pyrone moiety. In the HOMO-1 orbital indeed, the electronic density is strongly present on ring A while a certain degree of electron density is found on ring B (atoms $C_{2'}$, $C_{3'}$, $C_{4'}$, and $C_{5'}$) and in the bond between rings C and B. The LUMO and LUMO+1 orbitals are characterized by a charge distribution involving the whole molecule (LUMO) and the rings A and C (LUMO+1).

Limited to the values in methanol available in literature (*38*), the agreement with our determinations appears to be satisfactory. The same agreement was found with the values computed by a previous theoretical work (*38*). In fact, we find that the most significant HOMO → LUMO transition band (band I) is localized at 385 and 388 nm, in methanol and in dimethylsulfoxide, respectively. This transition corresponds to a low charge transfer from the ring B to the ring A, mediated by the presence of the γ-pyrone ring. The second absorption band corresponding mainly to the HOMO-3 → LUMO and HOMO → LUMO+1

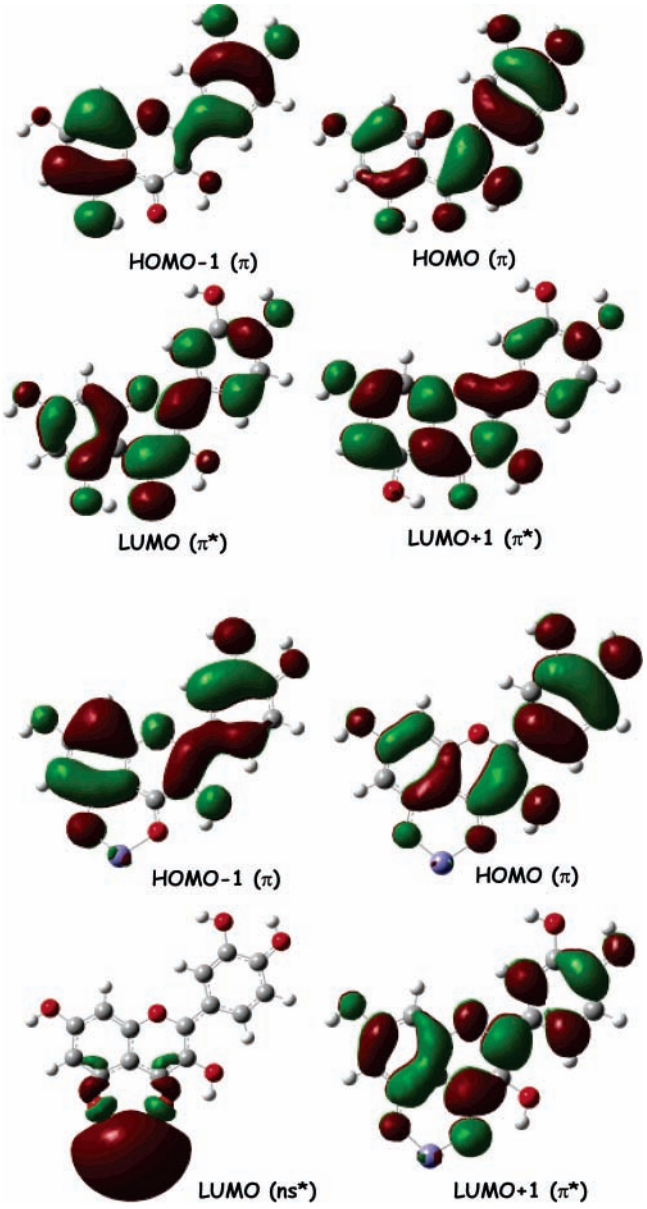

Figure 7. The four Gouterman's orbitals of quercetin (top) and its iron complex IVb (bottom).

transitions, is found at 267 (methanol) and 268 nm (DMSO). Finally, the HOMO → LUMO+3, HOMO-1 → LUMO+1, and HOMO-4 → LUMO transitions are localized at 244 nm, in both media.

The UV−vis spectrum also was recorded for the iron−quercetin monoanion complex in DMSO (*49*). For this reason, we have considered it interesting to simulate it theoretically.

The IVb lowest energy complex was chosen for this determination that we performed in both media considered before. Spectra were reported in **Figure 6**, vertical energies in **Table 3**, and molecular orbitals in **Figure 7**.

The HOMO → LUMO (band I) ligand-to-metal charge transfer (LMCT) transition falls at 453 (methanol) and 459 nm (DMSO). A significant band concerning the HOMO-1 → LUMO was localized at 387 and 392 nm in the two media, respectively.

Quantitative comparison cannot be made with the experimental spectrum in DMSO because it consists of an envelope not well resolved. However, taking into account the reliability of theoretical results obtained in the case of free quercetin, we can regard with confidence also the findings for its iron complex.

The HOMO → LUMO transition shows a very strong charge transfer from the quercetin ligand to the metallic center. The LUMO orbital, in fact, involves a large participation of the 3s atomic orbital of the iron cation. The HOMO-1 → LUMO transition at 387 nm shows the same features of the former.

The small differences concerning the localization of the single transitions in the two different media can be attributed to their polarity. In fact, as can be verified in the literature (*67*), an higher dielectric constant causes generally a shift of the transition at lower energy.

Conclusions. Iron(II) complexes of quercetin were studied by means of density functional based methods to give better insight into the "metals chelation mechanism" that this flavonoid can follow to perform its antioxidant properties. The study had the aim to elucidate the geometrical and electronic features of formed chelates, to determine the preferred coordination sites for Fe^{2+} and to identify the species that should be responsible for metal ion sequestration.

On the basis of the obtained results, we can draw the following considerations:

(i) Both neutral and deprotonated quercetin forms with iron(II) stable complexes. The 1:1 and 1:2 metal/ligand stoichiometries are possible in the complexes of the quercetin monoanion.

(ii) Binding energy values confirm that the 1:2 stoichiometry is the favored one.

(iii) Among the available positions present on neutral or anionic quercetin, oxygen atoms at the 3 and 4, and 5 and 4 carbons, seem to be the favored coordination sites for the iron cation. The behavior of Fe^{2+} was found to be similar to that shown by Al^{3+} but different from that of Pb^{2+}, which preferentially coordinates to the *o*-dihydroxy functionality.

(iv) The stability order of various complexes with bare cation depends on the formation of five- or six-membered rings. In particular, the presence of a six-membered ring introduces a greater stabilizing effect.

(v) Water molecules added to the complete iron coordination sphere influence the stability order of complexes also reducing the energetic gaps between them.

(vi) The high binding energy values indicate that quercetin is a powerful chelating agent that can sequester iron(II) in such a way to prevent its involvement in the Fenton reaction.

(vii) TDDFT methodologies can be successfully applied to obtain the UV−vis electronic spectra of free and complexed flavonoids, reproducing well the shape of the experimental ones.

LITERATURE CITED

(1) Hsieh, R. J.; Kinsella, J. E. Oxidation of polyunsaturated fatty acids: mechanisms, products, and inhibition with emphasis on fish. *Adv. Food Nutr. Res.* **1989**, *33*, 233−341.

(2) Kuhnau, J. The flavonoids. A class of semi-essential food components: their rolein human nutrition. *World Rev. Nutr. Diet.* **1976**, *24*, 117−191.

(3) Ko, F.; Chu, C.; Lin, C.; Chang, C.; Teng, C. Isoorientin-6-*O*-glucoside, a water-soluble antioxidant isolated from Gentiana arisanensis. *Biochem. Biophys. Acta.* **1998**, *1389*, 81−90.

(4) Novic, M.; Nikolovska, Z.; Solmajer, T. Quantitative structure-activity relationship of flavonoid $p56^{lck}$ protein tyrosine kinase inhibitors. A neural network approach. *J. Chem. Inf. Comput. Sci.* **1997**, *37*, 990−998.

(5) Amic, D.; Davidovic, D.; Juric, A.; Lucic, B.; Trinajstic, N. Structure-activity correlation of flavone derivatives for inhibition of cAMP phosphodiesterase. *J. Chem. Inf. Comput. Sci.* **1995**, *35*, 1034−1038.

(6) Uda, Y.; Price, K.; Williamson, G.; Rhodes, M. Induction of the anticarcinogenic marker enzyme, quinone reductase, in murine hepatoma cells in vitro by flavonoids. *Cancer Lett.* **1997**, *120*, 213−216.
(7) Tahara, S.; Katagiri, Y.; Ingham, J.; Mizutani, J. Prenylated flavonoids in the root of yellow lupin. *Phytochemistry* **1994**, *36*, 1261−1271.
(8) Amoros, M.; Simoes, C. M. O.; Girre, L.; Sauvager, F.; Cormier, M. Synergistic effect of flavones and flavonols against herpes simplex virus type 1 in cell culture. Comparison with the antiviral activity of propolis. *J. Nat. Prod.* **1992**, *55*, 1732−1740.
(9) Ng, T.; Huang, B.; Fong, W.; Yeung, H. Anti-human immunodeficiency virus (anti-HIV) natural products with special emphasis on HIV reverse transcriptase inhibitors. *Life Sci.* **1997**, *61*, 933−949.
(10) Merken, H. M.; Beecher, G. R. Measurement of food flavonoids by high-performance liquid chromatography: a review. *J. Agric. Food Chem.* **2000**, *48*, 578−599.
(11) Kawaii, S.; Tomono, Y.; Katase, E.; Ogawa, K.; Yano, M. Antiproliferative effects of the readily extractable fractions prepared from various *Citrus* juices on several cancer cell lines. *J. Agric. Food Chem.* **1999**, *47*, 2509−2512.
(12) Manthey, J. A.; Guthrie, N. Antiproliferative activities of *Citrus* flavonoids against six human cancer cell lines. *J. Agric. Food Chem.* **2002**, *50*, 5837−5843.
(13) Saija, A.; Scalese, M.; Lanz, M.; Marzullo, D.; Bonina, F.; Castelli, F. Flavanoids as antioxidant agents: importance of their interaction with biomembranes. *Free Rad. Biol. Med.* **1995**, *19*, 481−486.
(14) Miller, A. L. Antioxidant flavonoids: structure, function, and clinical usage. *Altern. Med. Rev.* **1996**, *1*, 103−111.
(15) Chang, W. S.; Lee, Y. J.; Lu, F. J.; Chiang, H. C. Inhibitory effects of flavonoids on xanthine oxidase. *Anticancer Res.* **1993**, *13*, 2165−2170.
(16) Chen, Y. T.; Zheng, R. L.; Jia, Z. J.; Ju, Y. Flavonoids as superoxide scavengers and antioxidants. *Free Radic. Biol. Med.* **1990**, *9*, 19−21.
(17) DeWhalley, C. V.; Rankin, J. F.; Rankin, S. M. Flavonoids inhibit the oxidative modification of low density lipoproteins. *Biochem. Pharmacol.* **1990**, *39*, 1743−1749.
(18) Skaper, S. D.; Fabris, M.; Ferrari, V. Quercetin protects cutaneous tissue-associated cell types including sensory neurons from oxidative stress induced by glutathione depletion: cooperative effects of ascorbic acid. *Free Radic. Biol. Med.* **1997**, *22*, 669−678.
(19) Della Loggia, R.; Ragazzi, E.; Tubaro, A. Anti-inflammatory activity of benzoppyrones that are inhibitors of cyclo- and lipo-oxygenase. *Pharmacol. Res. Commun.* **1988**, *20*, S91−S94.
(20) Kim, H. P.; Mani, I.; Ziboh, V. A. Effects of naturally-occurring flavonoids and biflavonoids on epiderman cyclooxygenase from guinea pigs. *Prostaglandins Leukot. Essent. Fatty Acids* **1998**, *58*, 17−24.
(21) Fox, C. C.; Wolf, E. J.; Kagey-Sobotka, A.; Lichtenstein, L. M. Comparison of human lung and intestinal mast cells. *J. Allergy Clin. Immunol.* **1988**, *81*, 89−94.
(22) Bronner, C.; Landry, Y. Kinetics of the inhibitory effect of flavonoids on histamine secretion from mast cells. *Agents Actions* **1985**, *16*, 147−151.
(23) Chaudry, P. S.; Cabera, J.; Juliani, H. R.; Varma, S. D. Inhibition of human lens aldose reductase by flavonoids, sulindac, and indomethacin. *Biochem. Pharmacol.* **1983**, *32*, 1995−1998.
(24) Kaul, T. N.; Middleton, E., Jr.; Ogra, P. L. Antiviral effect of flavonoids on human viruses. *J Med. Virol.* **1985**, *15*, 71−79.
(25) Wright, J. S.; Johnson, E. R.; Di Labio, G. A. Predicting the activity of phenolic antioxidants: theoretical method, analysis of substituent effects and application to major families of antioxidants. *J. Am. Chem. Soc.* **2001**, *123*, 1173−1183.
(26) Leopoldini, M.; Prieto Pitarch, I.; Russo, N.; Toscano, M. Structure, conformation and electronic properties of apigenin, luteolin and taxifolin antioxidants. A first principle theoretical study. *J. Phys. Chem. B* **2004**, *108*, 92−94.
(27) Leopoldini, M.; Marino, T.; Russo, N.; Toscano, M. Antioxidant properties of phenolic compounds. H-atom versus electron transfer mechanism. *J. Phys. Chem. B* **2004**, *108*, 4916−4922.
(28) Jovanovic, S. V.; Steenken, S.; Simic, M. G.; Hara, Y. In *Flavonoids in Health and Disease*; Rice-Evans, C.; Packer, L., Eds.; Marcel Dekker: New York, 1998; p 137.
(29) Brown, J. E.; Khodr, H.; Hider, R. C.; Rice-Evans, C. A. Structural dependence of flavonoid interactions with Cu^{2+} ions: implications for their antioxidant properties. *Biochem. J.* **1998**, *330*, 1173−1178.
(30) van Acker, S. A. B. E.; van den Berg, D. J.; Tromp, M. N. J. L.; Griffaen, D. H.; van Bennekom, W. P.; van Vijgh, W. J. F.; Bast, A. Structural aspects of antioxidant activity of flavonoids. *Free Radic. Biol. Med.* **1996**, *20*, 331−342.
(31) Schulz, J. B.; Lindenau, J.; Seyfried, J.; Dichganz, J. Glutathione, oxidative stress and neurodegeneration. *Eur. J. Biochem.* **2000**, *267*, 4904−4911.
(32) Murota, K.; Mitsukuni, Y.; Ichikawa, M.; Tsushida, T.; Miyamoto, S.; Terao, J. Quercetin-4′-glucoside is more potent than quercetin-3-glucoside in protection of rat intestinal mucosa homogenates against iron ion-induced lipid peroxidation. *J. Agric. Food Chem.* **2004**, *52*, 1907−1912.
(33) Heo, H. J.; Lee, C. Y. Protective effects of quercetin and vitamin C against oxidative stress-induced neurodegeneration. *J. Agric. Food Chem.* **2004**, *52*, 7514−7517.
(34) Kaldas, M. I.; Walle, U. K.; van der Woude, H.; McMillan, J. M.; Walle, T. Covalent binding of the flavonoid quercetin to human serum albumin. *J. Agric. Food Chem.* **2005**, *53*, 4194−4197.
(35) Rohn, S.; Rawel, H. M.; Kroll, J. Antioxidant activity of protein-bound quercetin. *J. Agric. Food Chem.* **2004**, *52*, 4725−4729.
(36) Hirota, S.; Takahama, U.; Ly, T. N.; Yamauchi, R. Quercetin-dependent inhibition of nitration induced by peroxidase/H_2O_2/nitrite systems in human saliva and characterization of an oxidation product of quercetin formed during the inhibition. *J. Agric. Food Chem.* **2005**, *53*, 3265−3272.
(37) Chien, J.-T.; Hsu, D.-J.; Chen, B.-H. Kinetic model for studying the effect of quercetin on cholesterol cxidation during heating. *J. Agric. Food Chem.* **2006**, *54*, 1486−1492.
(38) Cornard, J. P.; Dangleterre, L.; Lapouge, C. Computational and spectroscopic characterization of the molecular and electronic structure of the Pb(II)-quercetin complex. *J. Phys. Chem. A.* **2005**, *109*, 10044−10051.
(39) Leopoldini, M.; Marino, T.; Russo, N.; Toscano, M. Density functional computations of the energetic and spectroscopic parameters of quercetin and its radicals in the gas phase and in solvent. *Theor. Chem. Acc.* **2003**, *111*, 210−216.
(40) Erkoç, S.; Erkoç, F.; Keskin, N. Theoretical investigation of quercetin and its radical isomers. *Theochem* **2003**, *631*, 141−146.
(41) van Acker, S. A. B. E.; de Groot, M. J.; van der Berg, D.-J.; Tromp, M. N. J. L.; Kelder, D. G.-O.; van der Vijgh, W. J. F.; Bast, A. A quantum chemical explanation of the antioxidant activity of flavonoids. *Chem. Res. Toxicol.* **1996**, *9*, 1305−1312.
(42) Vasilescu, D.; Girma, R. Quantum molecular modelling of quercetin-Simulation of the interaction with the free radical *t*-BuOO. *Int. J. Quantum Chem.* **2002**, *90*, 888−902.
(43) Russo, N.; Toscano, M.; Uccella, N. Semiempirical molecular modelling into quercetin reactive site: structural, conformational, and electronic features. *J. Agric. Food Chem.* **2000**, *48*, 3232−3237.
(44) Mendoza-Wilson, A. M.; Glossmna-MitMik, G. CHIH-DFT determination of the molecular structure, infrared and ultraviolet spectra of the flavonoid quercetin. *Theochem* **2004**, *681*, 71−76.
(45) Cornard, J. P.; Merlin, J. C.; Boudet, A. C.; Vrielynck, L. Structural study of quercetin by vibrational and electronic spectroscopies combined with semiempirical calculations. *Biospectroscopy* **1997**, *3*, 183−193.

(46) Mira, L.; Fernandez, M. T.; Santos, M.; Rocha, R.; Florêncio, M. H.; Jennings, K. R. Interactions of flavonoids with iron and copper ions: A mechanism for their antioxidant activity. *Free Radic. Res.* **2002**, *36*, 1199−1208.

(47) Fernandez, M. T.; Mira, L.; Florêncio, M. H.; Jennings, K. R. Iron and copper complexation by angiotensin-converting enzyme inhibitors. A study by ultraviolet spectroscopy and electrospray mass spectrometry. *J. Inorg. Biochem.* **2002**, *92*, 105−111.

(48) Zhang, J.; Brodbelt, J. S.; Wang, J. Threshold dissociation and molecular modelling of transition metal complexes of flavonoids. *J. Am. Soc. Mass. Spectrom.* **2005**, *16*, 139−151.

(49) Bodini, M. E.; Copia, G.; Tapia, R.; Leighton, F.; Herrera, L. Iron complexes of quercetin in aprotic medium. Redox chemistry and interaction with superoxide anion radical. *Polyhedron* **1999**, *18*, 2233−2239.

(50) Satterfield, M.; Brodbelt, J. S. Enhanced detection of flavonoids by metal complexation and electrospray ionization mass spectrometry. *Anal. Chem.* **2000**, *72*, 5898−5906.

(51) Cornard, J. P.; Merlin, J. C. Spectroscopic and structural study of complexes of quercetin with Al(III). *J. Inorg. Biochem.* **2002**, *92*, 19−27.

(52) Frisch, M. J.; Trucks, G. W.; Schlegel, H. B.; Scuseria, G. E.; Robb, M. A.; Cheeseman, J. R.; Montgomery, J. A., Jr.; Vreven, T.; Kudin, K. N.; Burant, J. C.; Millam, J. M.; Iyengar, S. S.; Tomasi, J.; Barone, V.; Mennucci, B.; Cossi, M.; Scalmani, G.; Rega, N.; Petersson, G. A.; Nakatsuji, H.; Hada, M.; Ehara, M.; Toyota, K.; Fukuda, R.; Hasegawa, J.; Ishida, M.; Nakajima, T.; Honda, Y.; Kitao, O.; Nakai, H.; Klene, M.; Li, X.; Knox, J. E.; Hratchian, H. P.; Cross, J. B.; Adamo, C.; Jaramillo, J.; Gomperts, R.; Stratmann, R. E.; Yazyev, O.; Austin, A. J.; Cammi, R.; Pomelli, C.; Ochterski, J. W.; Ayala, P. Y.; Morokuma, K.; Voth, G. A.; Salvador, P.; Dannenberg, J. J.; Zakrzewski, V. G.; Dapprich, S.; Daniels, A. D.; Strain, M. C.; Farkas, O.; Malick, D. K.; Rabuck, A. D.; Raghavachari, K.; Foresman, J. B.; Ortiz, J. V.; Cui, Q.; Baboul, A. G.; Clifford, S.; Cioslowski, J.; Stefanov, B. B.; Liu, G.; Liashenko, A.; Piskorz, P.; Komaromi, I.; Martin, R. L.; Fox, D. J.; Keith, T.; Al-Laham, M. A.; Peng, C. Y.; Nanayakkara, A.; Challacombe, M.; Gill, P. M. W.; Johnson, B.; Chen, W.; Wong, M. W.; Gonzalez, C.; Pople, J. A. Gaussian, Inc., Pittsburgh, PA, 2003.

(53) Becke, A. D. J. The role of exact exchange. *Chem. Phys.* **1993**, *98*, 5648−5652.

(54) Lee, C.; Yang, W.; Parr, R. G. Development of the Colle-Salvetti correlation-energy formula into a functional of the electron density. *Phys. Rev. B* **1988**, *37*, 785−789.

(55) Ditchfield, R.; Hehre, W. J.; Pople, J. A. Self-consistent molecular-orbital methods: IX. An extended Gaussian-type basis for molecular-orbital studies of organic molecules. *J. Chem. Phys.* **1971**, *54*, 724−728.

(56) Hehre, W. J.; Ditchfield, R.; Pople, J. A. Self-consistent molecular orbital methods: XII. Further extensions of Gaussian-type basis sets for use in molecular orbital studies of organic molecules. *J. Chem. Phys.* **1972**, *56*, 2257−2261.

(57) Hariharan, P. C.; Pople, J. A. Accuracy of AH_n equilibrium geometries by single determinant molecular orbital theory. *Mol. Phys.* **1974**, *27*, 209−214.

(58) Gordon, M. S. The isomers of silacyclopropane. *Chem. Phys. Lett.* **1980**, *76*, 163−168.

(59) Hay, P. J.; Wadt, W. R. Ab Initio effective core potentials for molecular calculations *J. Chem. Phys.* **1985**, *82*, 270; 284; 299.

(60) Casida, M. E. *Recent Advances in Density Functional Methods, Part I*; Chong, D. P., Ed.; World Scientific: Singapore, 1995.

(61) Miertus, S.; Scrocco, E.; Tomasi, J. Electrostatic interaction of a solute with a continuum. A direct utilization of ab initio molecular potentials for the prevision of solvent effects. *Chem. Phys.* **1981**, *55*, 117−129.

(62) Miertus, S.; Tomasi, J. Approximate evaluations of the electrostatic free energy and internal energy changes in solution processes. *Chem. Phys.* **1982**, *65*, 239−245.

(63) Cossi, M.; Barone, V.; Commi, R.; Tomasi, J. Ab initio study of solvated molecules: a new implementation of the polarizable continuum model. *Chem. Phys. Lett.* **1996**, *255*, 327−335.

(64) Barone, V.; Cossi, M.; Tomasi, J. A new definition of cavities for the computation of solvation free energies by the polarizable continuum model. *J. Chem. Phys.* **1997**, *107*, 3210−3221.

(65) Leopoldini, M.; Russo, N.; Toscano, M. Gas and liquid phase acidity of natural antioxidants. *J. Agric. Food Chem.* **2006**, *54*, 3078−3085.

(66) Deng, H.; Van Berkel, G. J. Electrospray mass spectrometry and UV/visible spectrophotometry studies of aluminum(III)-flavonoid complexes. *J. Mass Spectrom.* **1998**, *33*, 1080−1087.

(67) Cave, R. J.; Burke, K.; Castner, E. W., Jr. Theoretical investigation on the ground and excited states of coumarin 151 and coumarin 120. *J. Phys. Chem. A* **2002**, *106*, 9294−9305.

Received for review April 7, 2006. Revised manuscript received June 16, 2006. Accepted June 26, 2006. Financial support from the University of Calabria and Regione Calabria (POR Calabria 2000/2006 misura 3.16. d, progetto VACAVISS) is gratefully acknowledged.

JF060986H